



The Relationship between Nano Crystallite Structure and Internal Stress in Ni Coatings Electrodeposited by Watts Bath Electrolyte Mixed with Supercritical CO₂

V. C. Nguyen,^a C. Y. Lee,^{a,z} L. Chang,^{b,*} F. J. Chen,^{c,d} and C. S. Lin^c

^aDepartment of Mechanical Engineering, National Taipei University of Technology, Taipei 106, Taiwan

^bDepartment of Materials Science and Opto-electronic Engineering, National Sun Yat-Sen University, Kaohsiung 804, Taiwan

^cDepartment of Materials Science and Engineering and ^dDepartment of Mechanical Engineering, National Taiwan University, Taipei 106, Taiwan

In this study, the internal stress of Ni coating electroplated in the supercritical-CO₂ (Sc-CO₂) mixed Watts bath was investigated with a focus on the effects of plating parameters and additives. Both the internal stresses of the Ni coatings and their corresponding microstructures were examined. A relationship is found that the internal stress of the Ni coating was inversely proportional to its grain size and the Ni{200}/Ni{111} peak fraction in the measured X-ray diffraction pattern. The smaller grain size, accompanied with higher Ni{111} intensity, resulted in the higher internal stress of the coating, and vice versa. A proposed theoretical model, which took both the grain size and preferred crystalline orientation into account, correlated closely with experimental results in the internal stress. As a result, the presence of surfactant in the Sc-CO₂ electrolyte increased the internal stress of Ni coating. However, a reduction of internal stress is made possible by varying four factors: the raising of current density, the increasing of plating temperature, the lowering of plating pressure, and the addition of saccharin into electrolyte. A comparison to the internal stress of Ni coatings plated by the conventional method was also discussed in this study.

© 2012 The Electrochemical Society. [DOI: 10.1149/2.061206jes] All rights reserved.

Manuscript submitted January 12, 2012; revised manuscript received March 5, 2012. Published May 3, 2012.

Recently, the electrodeposition of nickel through the use of supercritical carbon dioxide (Sc-CO₂) electrolyte has been stated as a novel method for fabricating the nano-material products.¹⁻⁷ The special characteristics of the thus prepared nickel coatings include uniformity, high hardness, nano-sized grain, bright appearance, smooth surface, and high corrosion resistance. Thereby, the well penetration capability of the Sc-CO₂ mixed electrolyte/solution into complicated and narrow surface profile of plating template presents an advantageous strength in the fabrication of nano-sized electronic devices,⁸ which would be difficult to achieve with conventional methods. However, in our previous work,⁹ the internal stress of Sc-CO₂ Ni coating was found significantly higher than that of conventional one. In the coating applications, keeping the internal stress of a deposition under control is crucial for its structural integrity. Hence, there have been researches devoted to studying the underlined mechanisms as well as controlling the coating's internal stress. Some have reduced the internal stress of a coating by using additives such as saccharin in the electrolyte and/or controlling plating parameters.^{10,11}

There have been hypotheses proposed to explain the particular experimental observations in the internal stress accordingly. In the majority of these hypotheses, the following factors causing the change of deposit volume are considered: coalescence of crystallites, incorporation of hydrogen, occlusion of other foreign species, and generation of structural defects. The theory based on the crystallite joining has been postulated by Hoffman,¹² Nix and Clemens¹³ and Thompson.¹⁴ Basically, the theory suggested that the deposit forms first in a dispersed state and then recrystallizes. They assumed that when the individual crystallites grow, the attractive forces attempt to reduce the gap between them. However, because the constraint of the substrate does not allow any free displacement of the crystallites, a stress in the coating emerges. Moreover, microscopic observations established that this was also essentially true after the deposit became continuous.¹⁵ Consequently, the continuous coalescence of columnar grains with gaps between them is necessary for deposit thickening. Since the volume decrease is resulted from the joining of individual crystallites, one might expect a strong relationship between the internal stress and the parameters characterizing the deposit microstructure. In fact, the tie between grain size and stress, and the close relationship between

crystallographic orientation and stress have already been observed individually in the past.¹⁶⁻¹⁸ However, the combined effects have not yet been fully investigated, especially with Sc-CO₂ electrodeposited coatings. Therein, not only hydrogen, the CO₂ at supercritical state has also been incorporated/occluded into the Ni electrodeposits prepared by Sc-CO₂ method.⁹ Thus, the objective of this work is to study the probable correlation between the nano-crystalline Ni deposit and its generated internal stress. Subsequently, the interactive mechanism within the relationships would be addressed.

Experimental

Materials.— The compositions of Watts bath electrolyte and additives used for the nickel electrodeposition are listed in Table I. The non-ionic surfactant used in this work was polyoxyethylene sorbitan monolaurate (C₅₈H₁₁₄O₂₆). All the experimental chemicals were purchased from First Chemical Co. Ltd, Taiwan and employed in the electrodeposition without further refinement. Carbon dioxide with minimum purity of 99.9% was acquired from CC Gaseous Corp., Taiwan. The copper plate with dimensions of 7 mm wide, 30 mm long, and 0.1 mm thick, was employed as the working substrate. This long strip configuration was to facilitate the measurement of curvature in longitudinal direction while the effect of the curvature in the lateral direction could be minimized.

Experimental apparatus and method.— The schematic diagram of the Sc-CO₂ electroplating system used in this work is depicted in Fig. 1. The reaction chamber, which had a volume of ca.180 cc,

Table I. Compositions of the electrolyte used for nickel electrodeposition.

Chemicals	Concentrations
NiSO ₄ ·6H ₂ O, g/L	300
NiCl ₂ ·6H ₂ O, g/L	50
H ₃ BO ₃ , g/L	30
Surfactant, vol. %	0, 0.1, 0.5, 1.0, 1.5, 2.0
Saccharin, g/L	0, 0.1, 0.2, 0.5, 1.0, 2.0

* Electrochemical Society Active Member.

^z E-mail: leech@ntut.edu.tw

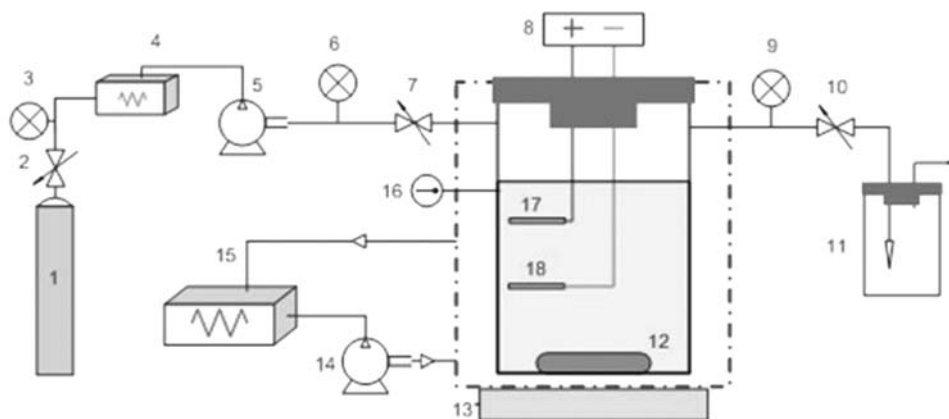


Figure 1. The experimental apparatus used for electroplating with an Sc-CO₂ mixed electrolyte. It is labeled as follows: 1. CO₂ cylinder; 2-7-10. Valve; 4. Cooler; 5. High pressure pump; 3-6-9. Pressure indicator; 8. Power supply; 11. Outlet electrolyte contain; 12. Stirring bar; 13. Agitator; 14. Water pump; 15. Hot water reservoir; 16. Thermometer; 17. Anode; 18. Cathode

was made of stainless steel with inner Teflon lining for electrical insulation and chemical inertness. The underneath magnetic agitator and a surrounding temperature controlled water jacket were used for mixing and maintaining the constant temperature of reaction chamber, respectively. Inside the reaction chamber, the cathode and anode were configured in horizontal orientation with a working distance of 20 mm for allowing adequate fluid sweeping on both electrode surfaces. The cathode was a copper substrate and the anode was a nickel plate of the same cross section area. Both the cathode and anode were connected to the bipolar DC power supply, BP4610 NF Corp., Japan, through titanium rods to the lead wires outside the chamber.

Prior to deposition, the polished copper substrate was treated sequentially in 10 wt% NaOH solution for degreasing, 10 wt% HCl solution for surface activating and then rinsed in de-ionized water. The cathode was masked and attached to a Teflon fixture with exposed electrode area about 200 mm². The electroplating solution was first put into the reaction chamber. With the chamber cap closed, liquid CO₂ was introduced into the chamber using a high pressure air driven liquid pump, Haskel DSF-60, U.S., and the chamber was pressurized to a predetermined pressure. The solution was then agitated with a magnetic stirrer at a speed of 400 rpm for at least 30 min. before the electroplating process, for solution stabilizing¹⁹ and cathode cleaning.²⁰

Each experiment was carried out with fresh solution in the planned plating parameters shown in Table II. After plating, the copper cathode with nickel coating was rinsed in deionized water then dried with warm stream of air. Before every examination and measurement, all samples were dry cleaned by Sc-CO₂.

Internal stress measurement.— After electrodeposition, the specimen geometrical configuration along the central line in the longitudinal direction was measured at seven equi-spaced locations using a laser displacement probe, KEYENCE LC-2440, Japan. The curvature of the plated specimen in the longitudinal direction was then determined by curve-fitting the configuration points with a circular arc

function. Furthermore, the average thickness of coating was calculated by the weight gain of the specimen after electroplating measured by an electronic balance, Mettler Toledo AB204, Switzerland, with a resolution of 0.1 mg. Accordingly, the internal stress of nickel coating was calculated by the Stoney equation, as shown in the following:²¹

$$\sigma_f = \frac{1}{6R} \frac{E_s t_s^2}{(1 - \nu_s) t_f} \quad [1]$$

where E_s and ν_s are the Young's modulus and Poisson's ratio of the substrate material, respectively. In Eq. 1, R is the measured radius of curvature, while t_s and t_f are the substrate and coating thicknesses, respectively. Additionally, in order to reduce the effect of exhausted hydrogen diffusion,²² the internal stress measurement was taken two hours after the specimen has been removed from the chamber.

Microstructural examination.— The average grain size of the deposit was measured by the X-ray Diffraction (XRD), Philips 1830/Mac, Netherlands, at a sweeping rate of 2 deg/min and calculated by the Scherrer equation with taking the broadening effect of the XRD machine into account. The X-ray was generated by a Cu-K α target operated at 30 kV and 20 mA with a wavelength of 0.15418 nm. In order to focus on the effect of crystalline structure on the internal stress of deposited coating, the curvature of deformed Ni coating and its corresponding grain size were both measured and calculated on the same specimen.

Results and Discussion

Fig. 2 presents the internal stresses of the nickel coatings prepared with Sc-CO₂ and conventional electroplating methods at different deposition thicknesses. All specimens were plated with the additive-free Watts bath solution under the condition of 14 MPa pressure, 30 vol.% CO₂, temperature of 60°C, and a current density of 0.02 A/cm². Specimens with different coating thicknesses were obtained by controlling the plating time. Because the cathodic efficiency of the Sc-CO₂ specimen was lower than the conventional one, slight difference in the coating thicknesses was observed for each plating time. As a result, the internal stresses of coatings were all in tensile mode and their magnitudes decreased as the thickness increased. This should be indebted to the diminishing structural mismatch and grain coarsening.²³ Clearly shown in Fig. 2 is the significantly higher internal stress for Sc-CO₂ electroplating than its conventional counterpart. The plausible mechanism has been reported and discussed in our previous work⁹ already. The effects of grain refinement, change in crystallographic orientation and the H₂/CO₂ charging will be discussed later.

Under the special characteristics of supercritical state, one can imagine that adjusting every plating parameter and electrolyte

Table II. Plating parameters used for the Ni electrodeposition.

Parameters	Values
CO ₂ fraction, vol.%	30
Pressure, MPa	8, 10, 12, 14, 16, 18
Temperature, °C	40, 45, 50, 55, 60, 65
Agitation, rpm	400
Current density, A/cm ²	0.005, 0.05, 0.1, 0.2, 0.3, 0.4, 0.5

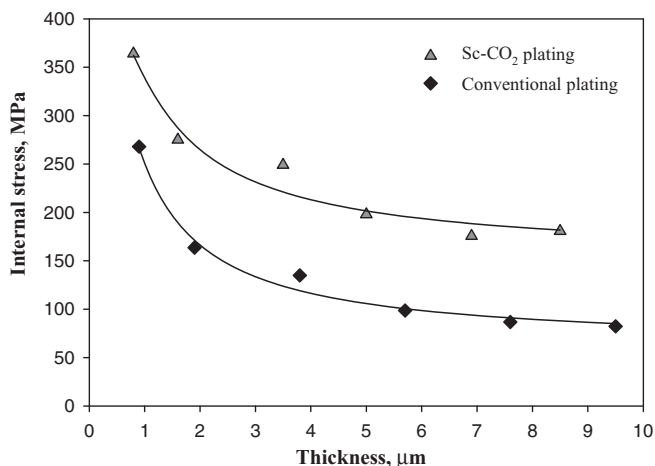


Figure 2. Internal stress of Ni coating plated in different thicknesses from additive-free Watt bath electrolyte by Sc-CO₂ and conventional methods, respectively.

composition probably alters the characteristics of the obtained electrodeposits. Therein, as mentioned in our previous work,⁹ an increase of CO₂ volume fraction in the reaction chamber introduces more CO₂ bubbles into the electrolyte and subsequently changes the size, concentration and/or its distribution in the aqueous plating solution. In fact, for a constant volume of reaction bath, the more fraction of CO₂ is equivalent to more soluble CO₂ bubbles in the electrolyte. With the same volume of solution and under the constant stirring speed, the more CO₂ bubbles inside electrolyte results in more exchanged covering rate on cathode surface. Hence, the addition of CO₂ bubbles in electrolyte apparently increases the periodic frequency. Once the on-time is initiated, more hydrogen is evolved when the pH has to be raised sufficiently so that the nickel electrodeposition can recommence.²⁴ Hence, the higher the periodic frequency, the more on-time beginnings appear per unit time. Therein, the ions have replenished and the nuclei re-formed at every short on-time interval. On the other hand, the shorter on-time interval has limited the growing duration of metal nucleus. Thus, the grains are refined and become one of the reasons for raising internal stress of Sc-CO₂ plating films.

The effect of plating pressure and temperature.— In Sc-CO₂ electroplating, the effects of pressure on grain size and internal stress of Ni coating are shown in Fig. 3. Note that, all the following results

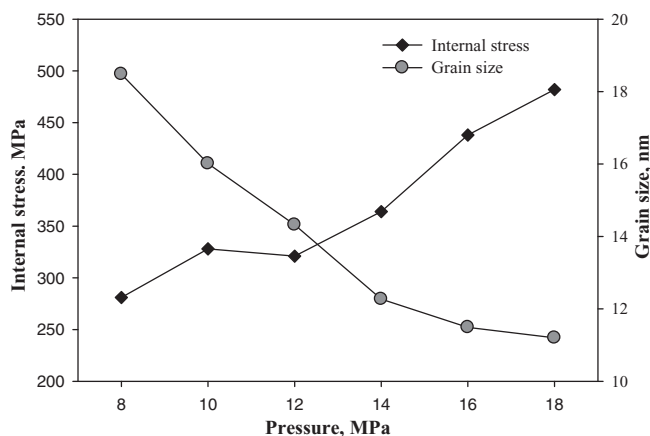


Figure 3. Effects of plating pressure on internal stress and grain size of Ni coating prepared by Sc-CO₂ electroplating. Plating condition: T = 60°C, CD = 0.02 A/cm².

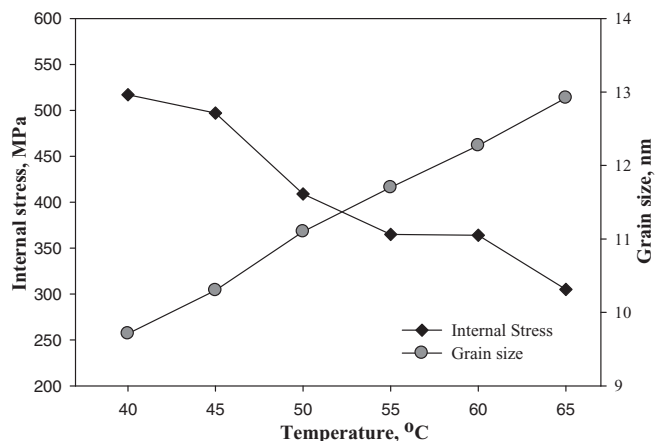


Figure 4. Effect of plating temperature on internal stress and grain size of Ni coating prepared by Sc-CO₂ electroplating. Plating condition: P = 14 MPa, CD = 0.02 A/cm².

were examined on the coating with approximate thickness of 1 μm. The results show that the higher the plating pressure, the finer the grains and the higher the internal stress. On the contrary, Fig. 4 shows the different effects of plating temperature on the internal stress of Ni coating. Herein, raising the plating temperature effectively decreased the internal stress while slightly increased the grain size of coating.

Under constant bath temperature, this pressure effect on the internal stress shows similar trend as that of CO₂ volume fraction's role. The result denotes that the higher plating pressure, the more CO₂ in reaction chamber and more dispersed CO₂ is introduced into electrolyte. Thus, the relevant effects of CO₂ in aqueous electrolyte are enhanced accordingly. More specifically, the higher plating pressure not only increases the CO₂ concentration but also reduces the size of CO₂ bubbles in the electrolyte.³ That explains the increase of electrical conductivity of the Sc-CO₂ solution when plating with higher pressure conditions.^{1,25} Thereby, both the increase of plating pressure as well as CO₂ volume fraction results in grains refinement. Accordingly, an increasing trend of internal stress with respect to the pressure was observed.

It is known that the energy of grain nucleus formation depends on the cathodic overpotential.²⁶ A large cathodic overpotential reduces the energy of nucleus formation, and therefore increases the nucleus densities.¹⁰ In Sc-CO₂ plating, the electrical conductivity of the electrolyte improves with the higher temperature. Thereby, the grain nucleation rate is reduced as a result of decreasing cathodic overpotential with increasing the bath temperature.^{23,27} On the other hand, at higher temperatures a faster surface diffusion of adatoms and nuclei causes an enhanced grain growth.^{28,29} Thus, raising plating temperature not only increases grain growth rate but also decreases nucleation rate. Both of them result in coarser grain and subsequently contribute to the lowering in the internal stress of the Ni coating, as depicted in Fig. 4.

The effect of plating current density.— Fig. 5 depicts the relationship between plating current density and internal stress of the Ni coatings. The result shows an increase in current density from 0.005 A/cm² to 0.2 A/cm² drastically decreased the internal stress from 500 MPa to 260 MPa. Further increase of current density just slightly reduced the internal stress of coating. The increase of current density in Sc-CO₂ electroplating has also been found to coarsen the grain size of Ni deposit in the work of Chang and Sone,³ and their results are included in Fig. 5 for comparison.

The XRD spectra of the coatings prepared with different current densities are also presented in Fig. 6. The results illustrate that the current density played an important role in controlling the Ni {200} peak intensity of the XRD pattern. Applying higher current density resulted in stronger Ni {200} peak intensity. On the other hand, the

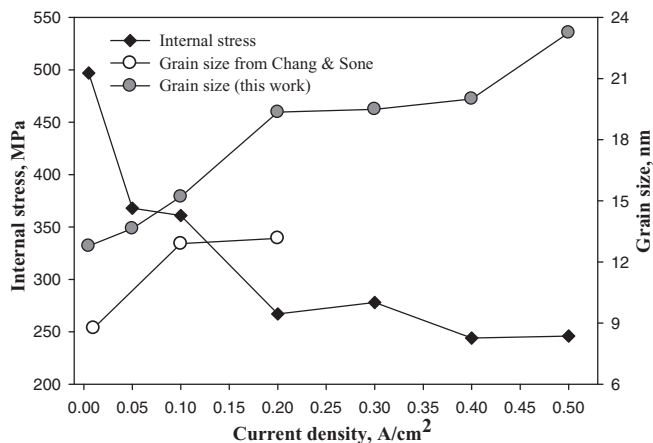


Figure 5. Effects of plating current density on internal stress and grain size of Ni coating prepared by Sc-CO₂ electroplating. Plating condition: T = 60°C, P = 14 MPa.

intensity of the Ni {111} peak showed little change. In this work, the average grain size of the coating was calculated through the diffraction peak corresponding to Ni {111}. To reduce the noise influence caused by relative thin coating, the peak parameters were determined after applying the nonlinear regression of Gaussian function and neglecting the influence of signal from copper substrate.

Clearly seen in Fig. 6 is that when increasing the plating current density, the intensity of Ni {200} crystallographic orientation was developed accordingly. In other words, the increase of current density resulted in a smaller fraction of Ni{111}/Ni{200}. This typical transition should be attributed to the fact that higher current density reduces concentration of Ni²⁺ at the electrode surface.²⁴ The lower ion density near cathode surface, again, reduces the nucleation rate and results in coarser grains. Hence, when the current density is increased, the more Ni {200} accompanying with coarser grain size subsequently lowers the internal stress of Ni coatings.

The effect of additives in the electrolyte.— The presence of surfactant in Sc-CO₂ mixed electrolyte increased the internal stress but the addition of saccharin in solution sharply decreased it, as shown in Fig. 7 and Fig. 8, respectively. Fig. 7 shows an addition of surfactant to 0.5 vol.% notably increased the internal stress. However, further

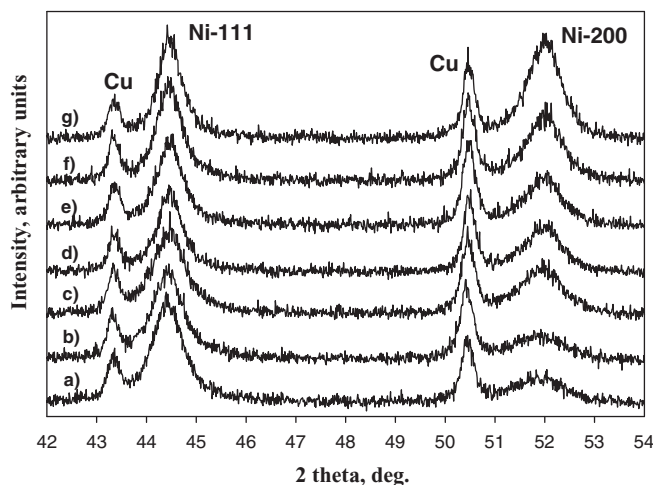


Figure 6. XRD patterns of Sc-CO₂ Ni coatings plated with different current densities: a) 0.005; b) 0.05; c) 0.1; d) 0.2; e) 0.3; f) 0.4; and g) 0.5 A/cm². Plating condition: T = 60°C, P = 14 MPa.

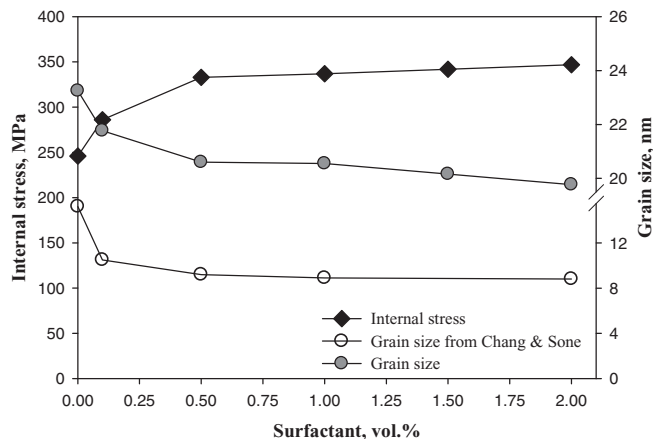


Figure 7. Effects of surfactant concentration on the internal stress and grain size of Ni coating prepared by Sc-CO₂ electroplating. Plating condition: T = 60°C, P = 14 MPa, CD = 0.5 A/cm².

increase of surfactant concentration seemed only to raise the internal stress insignificantly. In contrast, the addition of surfactant in Sc-CO₂ electrolyte resulted in finer grains. Similar effect of grain refinement from Chang & Sone³ was included in Fig. 7 for comparison. The difference between the grain sizes of this work and Chang & Sone's could be caused by the different surfactants used and the corrected grain size calculation by considering the broadening effect of the XRD measurement. Clearly shown in Fig. 7, again, is the inversely proportional relationship between the internal stress and the corresponding grain size of the Ni coating.

In Sc-CO₂ plating, the presence of surfactant in the electrolyte further improves the dispersion of CO₂ into aqueous electrolyte with smaller bubble size. Subsequently, the better homogenized electrolyte with smaller CO₂ bubbles shortens the on-time interval then limits the growing duration of metal nucleus. Therein, the ions have replenished and the nuclei re-formed at every short on-time interval. Thus, the Ni grains, again, are refined and the Ni coating possesses higher hardness as well as less pinhole⁷ on coating surface. The consistent trends of grain refinement in this work and Chang and Sone's result are depicted in Fig. 7. The result also shows the inversely proportional trend of the internal stress with respect to the grain size of coatings.

Meanwhile, as presented in Fig. 8, the addition of saccharin up to 2 g/L in the electrolyte continued to decrease both the internal stress of Ni deposit and its grain size.

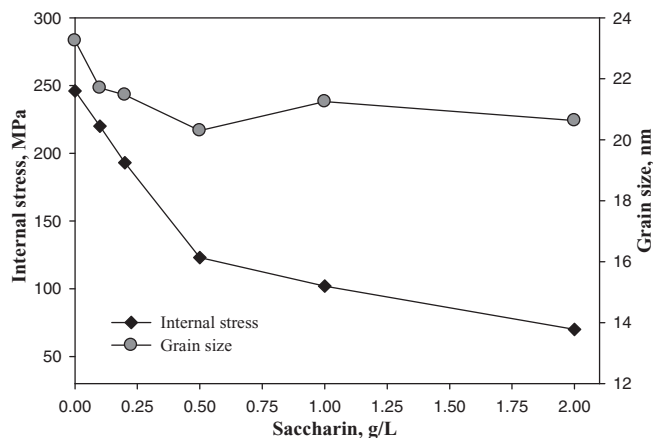


Figure 8. Effects of saccharin concentration on the internal stress and grain size of Ni coating prepared by Sc-CO₂ electroplating. Plating condition: T = 60°C, P = 14 MPa, CD = 0.5 A/cm².

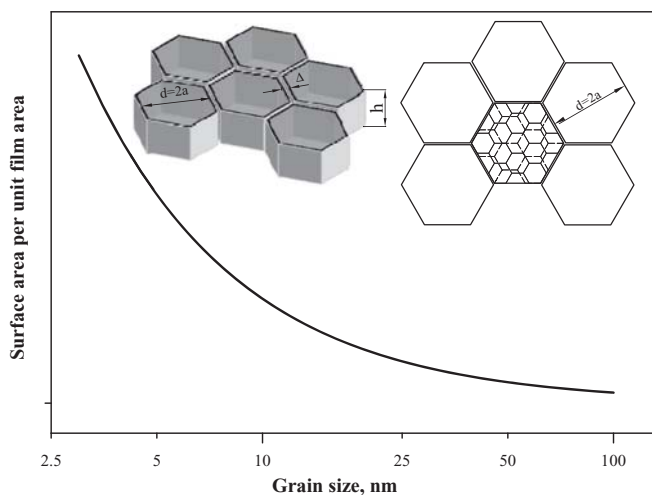


Figure 9. Relationship between surface area and grain size per unit film area, after Nix and Clemens' criteria.

There appears to be a general agreement, with both experimental and theoretical models, that saccharin is the organic additive playing the role of the internal stress reducer as well as grain refiner for the Ni electrodeposit.^{10,30–32} Actually, once saccharin presents in the plating electrolyte, its molecules are adsorbed on the cathode surface during electroplating. Consequently, by blocking the surface with the formation of complex compounds, which increases the frequency of nucleation and decreases the surface diffusion of nickel ions adsorbed on cathode surface, the saccharin retards the crystalline growth and finally results in grain refinement. Furthermore, the molecules are often incorporated into the metal deposit and the tensile stress is diminished accordingly. Thus, the reduction of internal stress and the refinement in grain size of Ni coating associated with the addition of saccharin in electrolyte herein again confirms its function in Sc-CO₂ metal electroplating. It is shown that the role of saccharin in Sc-CO₂ electroplating remains unchanged as in its conventional counterpart. The results shown in this work indicated the sensitive influences on the internal stress of Ni deposits from the Sc-CO₂ electroplating parameters as well as the addition of surfactant and saccharin into electrolyte. Herein, from the previous results presented in the aforementioned figures, there is evidence that the grain size and crystallite orientation have strong correlations with the internal stress of Ni coatings.

Relationship between crystallite structure and internal stress.— In order to determine the internal stress of thin film, Hoffman¹² started with the idea that crystallites snap together because the surface free energies are greater than the free energy of the grain boundary created by the coalescence. At coalescence of the individual grains, the overall energy of the system is lowered by reducing surface area, hence surface energy. Because of the elastic energy of the film substrate system, the interaction of the substrate does not allow any free displacement; hence, a tensile stress emerges in the film. The estimated stress of thin film is inversely proportional to its grain size value as clearly seen in Eq. 2:

$$\sigma = \frac{E}{1-\nu} \frac{\Delta}{d} \quad [2]$$

where $E/(1-\nu)$ is the biaxial modulus of the film and d is the grain size, Δ is the gap between adjacent crystallites, as illustrated in Fig. 9.

By considering this criterion, Nix and Clemens¹³ have figured out the distribution of crystals in a specific film area with hexagonal crystallites growing on a substrate. Generally, polycrystalline film is formed through the nucleation of isolated crystals on a substrate surface. Coalescence of the islands is one of the mechanisms employed to explain the occurrence of tensile stress. By joining two formerly

separated grains together, two times the surface energy is traded for the grain boundary energy. This effect should be operative from the beginning of coalescence to the formation of a continuous film. Once a continuous film has been formed through nucleation, growth, and coalescence process, thickening is normally expected to occur via epitaxial growth on pre-existing grains. Practically, Steel et al.¹⁵ had experimented and obtained a good correlation between the buildup of the tensile stress and the coalescence of the film. Thereby, the surface energy of isolated crystallites before coalescence can be estimated by:

$$E_1 = E_0 + \frac{2h\gamma_{sv}}{a} \quad [3]$$

where E_0 is the free energy per unit film area associated with both the top surface of the film and the film/substrate interface, and the second term represents the free energy of the side faces of the crystallites, per unit film area. The term γ_{sv} represents for the surface free energy of the crystallites. By applying Eq. 3 with a consideration of varying grain diameter within a specific unit film area, the distribution of estimated surface area associated with grain size is depicted in Fig. 9. Herein, by taking the gap between Ni adjacent crystals into account, $\Delta = 0.249$ nm,³³ only the results corresponding to grains larger than 3 nm were plotted. As a result, in a specific unit film area, the smaller grains that possess more surface area would be able to generate higher surface energy accordingly. After coalescence, the free energy per unit film area becomes¹³

$$E_2 = E_0 + \frac{h\gamma_{gb}}{a} + \frac{E}{1-\nu} h \left(\frac{\Delta}{2a} \right)^2 \quad [4]$$

where the second term is the grain boundary free energy and the third term is the strain energy per unit film area. The crystallites are assumed to be elastic and isotropic with Young's modulus E and Poisson's ratio ν . By setting $E_2 - E_1 = 0$, Nix and Clemens had derived the following equation for estimating the stress in the film:

$$\sigma_{\max} = \left[\frac{(2\gamma_{sv} - \gamma_{gb})}{a} \frac{E}{1-\nu} \right]^{\frac{1}{2}} \quad [5]$$

Eq. 4 denotes that the smaller grain possesses higher surface free energy. Thus, crystallite coalescence can lead to the higher tensile stresses in the film, Eq. 5. For grains in the order of 10 nm, crystallite coalescence can be sufficiently high for driving the development of stresses in the grains on the order of GPa.¹³ This relationship has been also observed in the electrodeposited iron-nickel alloy film.¹⁷

On the other hand, the film coarsening, coalescence, and grain growth characteristics depend on its size as well as on the crystallographic orientation of a grain relative to that of its neighbors.²³ When two adjacent grains possess different crystallographic orientations, the boundary that connects the two adjacent crystalline grains has energy of its own. That energy depends on the orientation differences of the two adjacent grains. The greater mismatch between adjacent grains, the higher grain boundary energy at the surface of the boundaries.

Moreover, for monocrystalline metal, the Young's moduli in different lattice directions are different. Young's modulus of Ni{111} is 303 GPa, the highest value comparing to 137 GPa and 233 GPa for Ni{100} and Ni{110}, respectively.³³ Additionally, the strain energy density of {111} texture film is higher than that of the {100}.²³ Through experiments, Rahman et al.³⁴ proved that the Young's modulus of Ni film plated through Sc-CO₂ method is higher than that of the conventional one. These likely relate to the higher tensile internal stress in the {111} texture film previously observed.^{18,35} In this work, the transition of crystallite orientation associated with varying internal stress is clearly observed, as depicted in Fig. 6, when Ni{200} intensity developed with increasing current density.

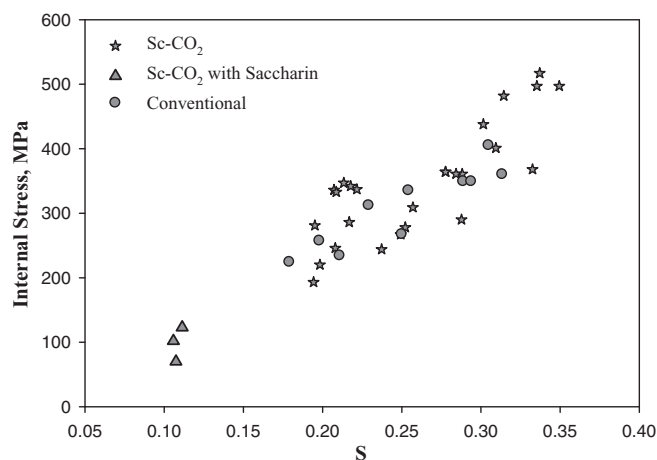


Figure 10. Crystal structure and Internal stress relationship of Ni electrodeposits: $K = 2.5$ for conventional results, $K = 1.0$ for the Sc-CO₂ results, and $K = 0.5$ for the results of Saccharin effects. Films' thicknesses are approximate to 1 μm .

By taking the effect of crystallographic orientation into account, Eq. 5 can be modified as:

$$\sigma_{\max} = \left[\frac{(2\gamma_{sv} - \gamma_{gb})^{\frac{1}{2}}}{a^{\frac{1}{2}}} \right] \left[\frac{E}{1 - \nu} \frac{I_{111}}{I_{111} + I_{200} + I_{220} + I_{311}} \right]^{\frac{1}{2}} \quad [6]$$

where I_{hkl} is intergrated intensity of the $\{hkl\}$ diffraction peak. The first bracket term denotes for the effect of surface and grain boundary energies associated with its grain size and the second one considers for the effect of anisotropic Young's modulus of the coating associated with crystallographic orientation of grains. In order to correlate this criterion with the experimental results, a parameter S is distilled from Eq. 6:

$$S = \left[\frac{K}{a^{\frac{1}{2}}} \right] \left[\frac{I_{111}}{I_{111} + I_{200}} \right]^{\frac{1}{2}} \quad [7]$$

In the above equation, S is defined as an internal stress parameter, which accounts for both effects of grain size and its crystallographic orientation. In the meantime, K is the constant accommodates for the difference between surface energy and grain boundary energy per unit film area. By using the parameter S in Eq. 7, the measurements of the internal stress obtained from different plating methods are presented in Fig. 10. Because the coatings prepared from different methods may have different surface energy and grain boundary energy due to different defects and impurity solution elements, different K s need to be employed for different plating methods and material systems. In this work, $K = 2.5$ was applied for conventional method; $K = 1.0$ and $K = 0.5$ were implemented for Sc-CO₂ electroplating methods with and without the addition of saccharin into Watts bath electrolyte. With the chosen parameter S and K s, the results in Fig. 10 clearly show the internal stress of the coating is closely related to the parameter S .

In the conventional nickel electroplating results, the incorporation of hydrogen around grain boundaries (1–2 nm) had been observed through the TEM micrograph.³⁶ Once the occluded hydrogen diffused and escaped from the coating, the tensile internal stress was increased accordingly.^{16,32} In the Sc-CO₂ electroplating, as mentioned previously, H₂/CO₂ was occluded into electrodeposits during plating. The inclusion of more H₂/CO₂ bubbles around grain boundaries increases the grain boundary energy of coating.³⁷ Moreover, the surface energy of Ni {111} is smaller than those of Ni {100} and Ni {110}.³⁸ Thus, the Sc-CO₂ nickel coatings that possess less Ni {200} than the conventional ones^{6,7,9} should have lower surface energy. By referring to the definition of K , i.e. the difference between surface energy and grain boundary energy, a smaller K for Sc-CO₂ plating than conventional

one becomes reasonable. However, it should be noted that the effect of the grain refinement of Sc-CO₂ nickel coatings over conventional ones still prevails and causes the higher internal stress in the Sc-CO₂ coatings presented in Fig. 2.

Furthermore, the internal stress of Sc-CO₂ nickel coatings prepared with the presence of saccharin in plating electrolyte should be elucidated as well. As mentioned previously, the saccharin in the electrolyte is usually co-deposited into coating. Once Saccharin is deposited into coating, the molecules that locate around the grain boundaries play the role as the foreign substance incorporation for lowering tensile internal stress. The mechanism discussed here is similar to that of compressive stress generation suggested by Hearne and Floro.³⁹ On the other hand, impurity-induced suppression of grain growth during deposition can lead to an increase in the grain boundary energy per volume.²³ Hence, the grain boundary energy might be increased with the incorporation of saccharin molecules in Ni coating. This can further decrease the parameter K comparing with that of Sc-CO₂ plating without saccharin. Thus, the more saccharin concentration in electrolyte, the higher incorporated density in the coating. Consequently, the measured internal stress fits better with lower K , as clearly observed by the three isolated triangle points in Fig. 10, in which the electrolyte were prepared with high saccharin concentration.

Conclusions

The experimental results in this work indicated that the internal stress of the Ni deposit was sensitive to the parameters employed in the Sc-CO₂ electroplating process. The relationship between the microstructure characteristics, mainly grain size and crystallographic orientation, and the internal stress of nickel electrodeposits, established with the proposed theoretical model, has correlated well to the measurements. Furthermore, the higher plating pressure and the presence of surfactant in electrolyte increased the internal stress of the Ni coating, respectively. Nevertheless, the internal stress of the coating can be reduced by raising plating temperature, and increasing the current density. Finally, the effects of saccharin in Sc-CO₂ electroplating on refining grains and reducing tensile stress remain unchanged over in its conventional counterpart.

Acknowledgments

The partial financial support from National Science Council, Taiwan under the grant No. NSC 98-2221-E-027 -083 -MY3 is gratefully acknowledged.

References

- H. Yoshida, M. Sone, A. Mizushima, H. Yan, H. Wakabayashi, K. Abe, X. T. Tao, S. Ichihara, and S. Miyata, *Surf. Coat. Technol.*, **173**, 285 (2003).
- H. Wakabayashi, N. Sato, M. Sone, U. Takada, H. Yan, K. Abe, K. Mizumoto, S. Ichihara, and S. Miyata, *Surf. Coat. Technol.*, **190**, 200 (2005).
- T. F. M. Chang and M. Sone, *Surf. Coat. Technol.*, **205**, 3890 (2011).
- T. F. M. Chang, M. Sone, A. Shibata, C. Ishiyama, and Y. Higo, *Electrochimica Acta*, **55**, 6469 (2010).
- H. Yan, M. Sone, A. Mizushima, T. Nagai, K. Abe, S. Ichihara, and S. Miyata, *Surf. Coat. Technol.*, **187**, 86 (2004).
- S. T. Chung, H. C. Huang, S. J. Pan, W. T. Tsai, P. Y. Lee, C. H. Yang, and M. B. Wu, *Corros. Sci.*, **50**, 2614 (2008).
- S. T. Chung and W. T. Tsai, *J. Electrochem. Soc.*, **156**, D457 (2009).
- A. H. Romang and J. J. Watkins, *Chem. Rev.*, **110**, 459 (2010).
- V. C. Nguyen, C. Y. Lee, F. J. Chen, C. S. Lin, and T. Y. Liu, *Surf. Coat. Technol.*, **206-14**, 3201 (2012).
- A. M. Rashidi and A. Amadeh, *Surf. Coat. Technol.*, **204**, 353 (2009).
- Y. Xuetao, W. Yu, S. Dongbai, and Y. Hongying, *Surf. Coat. Technol.*, **202**, 1895 (2008).
- R. W. Hoffman, *Thin Solid Films*, **34**, 185 (1976).
- W. D. Nix and B. M. Clemens, *J. Mater. Res.*, **14-8**, 3467 (1999).
- C. V. Thompson and R. Carel, *J. Mech. Phys. Solids*, **44-5**, 657 (1996).
- S. C. Steel, C. V. Thompson, S. J. Hearne, and J. A. Floro, *J. Appl. Phys.*, **88**, 7079 (2000).
- C. S. Lin, C. Y. Lee, F. J. Chen, and W. C. Li, *J. Electrochem. Soc.*, **152-6**, 370 (2005).
- F. Czerwinski, *J. Electrochem. Soc.*, **143-10**, 3327 (1996).
- L. Chang, C. H. Chen, and H. Fang, *J. Electrochem. Soc.*, **155-1**, D57 (2008).

19. S. R. P. d. Rocha, P. A. Psathas, E. Klein, and K. P. Johnston, *J. Colloid Interface Sci.*, **239**, 241 (2001).
20. H. Yoshida, M. Sone, A. Mizushima, K. Abe, X. T. Tao, S. Ichihara, and S. Miyata, *Chem. Lett.*, **020579**, 1086 (2002).
21. G. C. A. M. Janssen, M. M. Abdalla, F. van Keulen, B. R. Pujada, and B. van Venrooy, *Thin Solid Films*, **507**, 1858 (2009).
22. S. J. Hearne and J. A. Floro, *J. Appl. Phys.*, **97**, 014901.1 (2005).
23. C. V. Thompson, *Annu. Rev. Mater. Sci.*, **30**, 159 (2000).
24. A. M. El-Sherik, U. Erb, and J. Page, *Surf. Coat. Technol.*, **88**, 70 (1996).
25. M. S. Kim, J. Y. Kim, C. K. Kim, and N. K. Kim, *Chemosphere*, **58**, 459 (2005).
26. E. Budevski, G. Staikov, and W. J. Lorenz, *Electrochimica Acta*, **45**, 2559 (2000).
27. H. Natter and R. Hempelmann, *Z. Phys. Chem.*, **222**, 319 (2008).
28. H. Natter, M. Schmelzer, and R. Hempelmann, *J. Mater. Res.*, **13**, 1186 (1998).
29. J. X. Kang, W. Z. Zhao, and G. F. Zhang, *Surf. Coat. Technol.*, **203**, 1815 (2009).
30. R. Weil, *Plating*, **57**, 1231 (1970) and **58**, 50–56, 137–146 (1971).
31. S. H. Kim, H. J. Sohn, Y. C. Joo, Y. W. Kim, T. H. Yim, H. Y. Lee, and T. Kang, *Surf. Coat. Technol.*, **199**, 43 (2005).
32. S. Armyanov and G. S. Chakarova, *J. Electrochem. Soc.*, **139**, 3454 (1992).
33. M. A. Meyers and K. K. Chawla, *Mechanical Behavior of Materials* P. 275, Prentice Hall, New Jersey, US, 1999.
34. Md. Z. Rahman, M. Sone, M. Eguchi, K. Ikeda, S. Miyata, and T. Yamamoto, *International Conference on Mechanical Engineering*, pp. 28–30 (Dec, 2005).
35. S. P. Kim, H. M. Choi, and S. K. Choi, *Thin Solid Films*, **322**, 298 (1998).
36. F. D. Torre, H. V. Swygenhoven, and M. Victoria, *Acta Materialia*, **50**, 3957 (2002).
37. Y. Y. Huang, Y. C. Zhou, and Y. Pan, *Physica. B*, **405**, 1335 (2010).
38. L. Vitos, A. V. Ruban, H. L. Skriver, and J. Kollár, *Surface Science*, **411**, 186 (1998).
39. S. J. Hearne and J. A. Floro, *J. Appl. Phys.*, **97**, 014901.1 (2005).